Nanometer-Scale Dielectric Self-assembly Process for Anode Modification in Organic Light-Emitting Diodes. Consequences for Charge Injection and Enhanced Luminous Efficiency

Joshua E. Malinsky,[†] Jonathan G. C. Veinot,[†] Ghassan E. Jabbour,*[,‡] Sean E. Shaheen,[‡] Jeffrey D. Anderson,[§] Paul Lee,[§] Andrew G. Richter,[†,||] Alexander L. Burin,[†,||] Mark A. Ratner,*[,†] Tobin J. Marks,*[,†] Neal R. Armstrong,*[,§] Bernard Kippelen,*[,‡] Pulak Dutta,*[,||] and Nasser Peyghambarian*[,‡]

Department of Chemistry and the Materials Research Center, and Department of Physics and Astronomy and the Materials Research Center, Northwestern University, Evanston, Illinois 60208-3113, and Optical Sciences Center, and Department of Chemistry, University of Arizona, Tucson, Arizona 85721

Received March 26, 2002

Layer-by-layer, self-limiting chemisorptive siloxane self-assembly using $Si_3O_2Cl_8$ as the precursor affords thin, conformal, relatively dense, largely pinhole-free dielectric films that can be deposited on oxide surfaces with sub-nanometer control of film thickness (8.3(1) Å/layer). Deposition chemistry, microstructure, and hole injection/work function modification properties of these $(SiO_2)_x$-like films on single-crystal Si(111) and polycrystalline indium tin oxide (ITO) substrates have been characterized by synchrotron specular X-ray reflectivity, cyclic voltammetry, X-ray and UV photoelectron spectroscopy, and atomic force microscopy. Chemisorption of these $(SiO_2)_x$ films onto the ITO anodes of three-layer, vapor-deposited organic electroluminescent devices (ITO/$(SiO_2)_x$/TPD/Alq/Al) nearly triples the external quantum and luminous efficiencies. The efficiency enhancement is attributed to hole and electron injection fluence balance caused by modification of the effective voltage profile brought about by the assembly of well-ordered siloxane layers. Interestingly, as a function of increasing $(SiO_2)_x$ layer thickness, device turn-on voltage first increases ($x = 0 \rightarrow 1$), progressively decreases ($x = 1 \rightarrow 2 \rightarrow 3$), and then increases ($x = 3 \rightarrow 4$). A theoretical model based upon computation at the ab initio level is proposed in which the self-assembled dielectric layers induce an additional, thickness-dependent "built-in" electric field across the organic transport layers, thereby simultaneously enhancing electron injection from the cathode (increasing luminescence efficiency) and decreasing the efficiency of hole injection (changing the turn-on voltage).

Introduction

Following initial reports by Tang and VanSlyke[1] of vapor-deposited thin-film organic light-emitting diodes (OLEDs),[2] intense research activity has focused on understanding microstructure−luminescence relationships and on enhancing the operating performance characteristics of such devices. These studies reflect the fundamental challenge of understanding charge transport and luminescence in bulk molecular and macromolecular solids as well as across interfacial regions present in such structures.[2,3] Additionally, an important technological driving force has been to ultimately incorporate these materials and heterostructures into a host of monochrome and full color display systems. These applications require organic materials to afford heterostructures capable of operating at low voltages, with high emissive quantum efficiencies, for a variety

* To whom correspondence should be addressed.
[†] Department of Chemistry and the Materials Research Center, Northwestern University.
[‡] Optical Sciences Center, University of Arizona.
[§] Department of Chemistry, University of Arizona.
[||] Department of Physics and Astronomy and the Materials Research Center, Northwestern University.

(1) Tang, C. W.; VanSlyke, S. A. *Appl. Phys. Lett.* **1987**, *51*, 913−917.

(2) For recent reviews and overviews of this field, see: (a) Kowalsky, W.; Becker, E.; Benstem, T.; Johannes, H.-H.; Metzdorf, D.; Neuner, H.; Schobel, J. *Adv. Solid State Phys.* **2000**, *40*, 795−808. (b) Baldo, M. A.; Thompson, M. E.; Forrest, S. R. *Pure Appl. Chem.* **1999**, *71*, 2095−2106. (c) Kraft, A.; Grimsdale, A. C.; Holmes, A. B. *Angew. Chem., Int. Ed. Engl.* **1998**, *37*, 402−428. (d) Epstein, A. J., Yang, Y., Eds. *MRS Bull.* **1997**, June, 13−56, and articles therein. (e) Burrows, P. E.; Gu, G.; Bulovic, V.; Shen, Z.; Forrest, S. R.; Thompson, M. E. *IEEE Trans. Electron. Devices* **1997**, *44*, 1188.

(3) (a) Friend, R. H.; Gymer, R. W.; Holmes, A. B.; Burroughes, J. H.; Marks, R. N.; Taliani, C.; Bradley, D. D. C.; Dos Santos, D. A.; Bredas, J. L.; Logdlund, M.; Salaneck, W. R. *Nature* **1999**, *397*, 121−128. (b) Ishii, H.; Sugiyama, K.; Ito, E.; Seki, K. *Adv. Mater.* **1999**, *11*, 605. (c) Hung, L. S.; Tang, C. W. *Appl. Phys. Lett.* **1999**, *74*, 3209−3211. (d) Lee, H. S.; Kho, S. I.; Chung, T. G.; Kim, T. W.; Lee, W. J.; Kang, D. Y. *Mol. Cryst. Liq. Cryst. Sci. Technol. Sect. A-Mol. Cryst. Liq. Cryst.* **1999**, *327*, 189−192. (e) Lee, S. T.; Gao, Z. Q.; Hung, L. S. *Appl. Phys. Lett.* **1999**, *75*, 1404−1406. (f) Jabbour, G. E.; Kawabe, Y.; Shaheen, S. E.; Wang, J. F.; Morrell, M. M.; Kippelen, B.; Peyghambarian, N. *Appl. Phys. Lett.* **1997**, *71*, 1762−1764. (g) Han, E. M.; Do, L. M.; Yamamoto, N.; Fujihira, M. *Chem. Lett.* **1995**, 57−58.

10.1021/cm020293q CCC: $22.00
Published on Web 06/12/2002

of colors, with sufficiently long device lifetimes.[2e,4] The basic fabrication of OLED structures involves creating molecular/macromolecular layers sandwiched between a transparent conductive oxide anode such as indium tin oxide (Sn-doped bixbyite In_2O_3; ITO) and a low work function metal cathode via vapor or solution phase deposition.[2,5] Injected electrons and holes migrate (predominantly via disorder-modulated hopping mechanisms[6]) through the interposed organic layers to recombine radiatively within the emissive layer. Efficient performance of such devices requires maximum and balanced fluence of injected holes and electrons. Such a balance of injected charge minimizes the number of carriers that migrate unproductively to the opposite electrode without radiatively recombining, hence reducing the luminous efficiency and simultaneously risking layer degradation.[2] Of equal importance is electron−hole recombination in a region sufficiently remote from the electrode to avoid quenching of emissive excitons.[2,7,8]

At each metal/semiconductor−organic interface, a barrier to charge injection exists that is poorly understood but doubtless dependent upon, among other factors, atomic scale microstructural details and the energetic alignment of the electrode Fermi levels with the HOMO or LUMO of the hole transport layer (HTL) or electron transport layer (ETL), respectively.[2,4,6,9−12] It has recently been observed that OLED response characteristics (quantum efficiency, turn-on voltage, and device robustness) can be dramatically altered by nanoscale modification of the electrode−organic interface and via mechanisms that are in a great many cases incompletely defined.[3f,5b,13,14] Modifications to the ETL−metal cathode interface are variously postulated to increase the electron injection fluence into the ETL, to prevent migration of cathode metal ions into the ETL,[3f,5b,13e] and to provide buffer layers to protect the ETL from sputter damage during cathode deposition.[3c] Likewise, the ITO−HTL interface has also been subjected to extensive empirical manipulation. Recent reports describe ITO surface modification by oxidative/protic chemical treatment, oxide overlayer physical vapor deposition, metal deposition, and amphiphile/polymer/monolayer chemisorption.[3a,b,13,15] Details of the resulting interface structure(s) (e.g., contiguity, thickness, smoothness, microstructure, cohesion, and pinhole density) and mechanism(s) of action have generally been difficult to characterize; however, altering interfacial electric fields,[10,13e] balancing electron/hole injection fluences,[14] reducing injected charge backscattering,[13i] confining electrons in the emissive layer,[13k] and minimizing anode Fermi level−HTL HOMO energetic discontinuities[13d,j,k] have all been proposed. In each case, varying degrees of improved device performance such as lower turn-on voltage, greater thermal stability, and/or higher quantum efficiency have been reported. Recent studies in this laboratory with self-assembled arylamine hole transport/injection monolayers suggests that one major function of these, and by implication, similar ultrathin organic anode derivatization processes, is to stabilize the physical integrity of anode−HTL interfacial cohesion and ohmic contact by moderating the disparate surface energies.[13a,b]

In an effort to better understand the aforementioned anode functionalization effects, we sought a means by which to deposit ultrathin, structurally precise, covalently bound anode coatings. In this contribution, we present a full discussion of layer-by-layer, self-limiting chemisorptive siloxane self-assembly techniques[14,16,17,18] to introduce smooth, robust, conformal, contiguous, microstructurally/electronically well-defined dielectric layers of controllable dimensions at the ITO anode−HTL interface of conventional three-layer, vapor-deposited OLED devices.[14] Applying diverse physicochemical characterization techniques, we show that this

(4) Roitman, D. B.; Antoniadis, H.; Sheats, J.; Pourmirzaie, F. *Optoelectron. World* **1998**, July, 163−168.

(5) (a) Hamada, Y.; Kanno, H.; Sano, T.; Fujii, H.; Nishio, Y.; Takahashi, H.; Usuki, T.; Shibata, K. *Appl. Phys. Lett.* **1998**, *72*, 1939−1941. (b) Li, F.; Tang, H.; Anderegg, J.; Shinar, J. *Appl. Phys. Lett.* **1997**, *70*, 1233−1235. (c) Adachi, C.; Nagai, K.; Tamoto, N. *Appl. Phys. Lett.* **1995**, *66*, 2679−2681.

(6) (a) Baldo, M. A.; Forrest, S. R. *Phys. Rev. B* **2001**, *64*, 5201−5219, and references therein. (b) Shen, Y.; Klein, M. W.; Jacobs, D. B.; Scott, J. C.; Malliaras, G. G. *Phys. Rev. Lett.* **2001**, *86*, 3867−3870, and references therein.

(7) Matsumura, M.; Ito, A.; Miyamae, Y. *Appl. Phys. Lett.* **1999**, *75*, 1042−1044.

(8) Burin, A. L.; Ratner, M. A. *J. Chem. Phys.* **1998**, *109*, 6092−6102.

(9) Yang, Y. in ref 2b, pp 31−38.

(10) Segura, J. L. *Acta Polym.* **1998**, *49*, 319−344.

(11) Jabbour, G. E.; Kippelen, B.; Armstrong, N. R.; Peyghambarian, N. *Appl. Phys. Lett.* **1998**, *73*, 1185−1187.

(12) Parker, I. D. *J. Appl. Phys.* **1994**, *75*, 1656−1666.

(13) (a) Cui, J.; Huang, Q.; Veinot, J. G. C.; Yan, H.; Marks, T. J. *Adv. Mater.* **2002**, *14*, 565−569. (b) Cui, J.; Huang, Q.; Wang, Q.; Marks, T. J. *Langmuir* **2001**, *17*, 2051−2054. (c) Ho, P. K. H.; Kim, J.-S.; Burroughes, J. H.; Becker, H.; Li, S. F. Y.; Brown, T. M.; Cacialli, F.; Friend, R. *Nature* **2000**, *404*, 481−484. (d) Appleyard, S. F. J.; Day, S. R.; Pickford, R. D.; Willis, M. R. *J. Mater. Chem.* **2000**, *10*, 169−173. (e) Piromreun, P.; Oh, H. S.; Shen, Y.; Malliaris, G. G.; Scott, J. C.; Brock, P. J. *Appl. Phys. Lett.* **2000**, *77*, 2403−2405. (f) Andersson, A.; Kugler, T.; Logdlund, M.; Holmes, A. B.; Li, X.; Salaneck, W. R. *Surf. Interface Anal.* **1999**, *28*, 186−190. (g) Carrard, M.; Goncalves-Conto, S.; Si-Ahmed, L.; Ades, D.; Siove, A. *Thin Solid Films* **1999**, *352*, 189−194. (h) Deng, Z. B.; Ding, X. M.; Lee, S. T.; Gambling, W. A. *Appl. Phys. Lett.* **1999**, *74*, 2227−2229.

(14) Preliminary observations were communicated previously: Malinsky, J. E.; Jabbour, G. E.; Shaheen, S. E.; Anderson, J. D.; Richter, A. G.; Marks, T. J.; Armstrong, N. R.; Kippelen, B.; Dutta, P.; Peyghambarian, N. *Adv. Mater.* **1999**, *11*, 227−231.

(15) (a) Shen, Y.; Jacobs, D. B.; Malliaris, G. G.; Koley, G.; Spencer, M. G.; Ioannidis, A. *Adv. Mater.* **2001**, *13*, 1234−1238. (b) Mason, M. G.; Hung, L. S.; Tang, C. W.; Lee, S. T.; Wong, K. W.; Wang, M. *J. Appl. Phys.* **1999**, *86*, 1688−1692. (c) Kurosaka, Y.; Tada, N.; Ohmori, Y.; Yoshino, K. *Synth. Met.* **1999**, *102*, 1101−1102. (d) Kurosaka, Y.; Tada, N.; Ohmori, Y.; Yoshino, K. *Jpn. J. Appl. Phys. Part 2-Lett.* **1998**, *37*, L872−L875. (e) Chao, C.-I.; Chuang, K.-R.; Chen, S.-A. *Appl. Phys. Lett.* **1996**, *69*, 2894−2896. (f) Gautier, E.; Lorin, A.; Nunzi, J.-M.; Schalchli, A.; Benattar, J.-J.; Vital, D. *Appl. Phys. Lett.* **1996**, *69*, 1071−1073. (g) Van Slyke, S. A.; Chen, C. H.; Tang, C. W. *Appl. Phys. Lett.* **1996**, *69*, 2160−2162.

(16) For introductions to this assembly approach, see: (a) van der Boom, M. E.; Richter, A. G.; Malinsky, J. E.; Dutta, P.; Marks, T. J. *Adv. Funct. Mater.* **2001**, *11*, 393−397. (b) Klaus, J. W.; Sneh, O.; George, S. M. *Science* **1997**, *278*, 1934−1936. (c) Lin, W.; Lee, T. L.; Lyman, P. F.; Lee, J. J.; Bedzyk, M. J.; Marks, T. J. *J. Am. Chem. Soc.* **1997**, *119*, 2205−2211. (d) Lin, W.; Lin, W. P.; Wong, G. K.; Marks, T. J. *J. Am. Chem. Soc.* **1996**, *118*, 8034−8042. (e) Ulman, A. *Chem. Rev.* **1996**, *96*, 1533−1554. (f) Marks, T. J.; Ratner, M. A. *Angew. Chem., Int. Ed. Engl.* **1995**, *34*, 155−173.

(17) (a) Whether or not chemisorptive siloxane-based assembly processes should be strictly classified as self-assembly remains open to discussion[17b] because the covalently bound layers form from noncovalently bound precursor assemblies,[17c] and packing motifs are largely dictated by noncovalent interactions.[16e,17c−e] (b) van der Veen, N. J.; Flink, S.; Deij, M. A.; Egberink, R. J. M.; van Veggel, F. C. J. M.; Reinhoudt, D. N. *J. Am. Chem. Soc.* **2000**, *122*, 6112−6113. (c) Richter, A. G.; Yu, C.-J.; Datta, A.; Kmetko, J.; Dutta, P. *Phys. Rev. E* **2000**, *61*, 607−615. (d) Wasserman, S. R.; Tao, T.-Y.; Whitesides, G. M. *Langmuir* **1989**, *5*, 1074−1087. (e) Moaz, R.; Sagiv, J. *Langmuir* **1987**, *3*, 1034−1044.

(18) (a) Evmenenko, G.; van der Boom, M. E.; Marks, T. J.; Dutta, P. *J. Chem. Phys.* **2001**, *115*, 6722−6727. (b) Malik, A.; Lin, W.; Durbin, M. K.; Marks, T. J.; Dutta, P. *J. Chem. Phys.* **1997**, *107*, 645−652. (c) Roscoe, S. B.; Kakkar, A. K.; Marks, T. J.; Malik, A.; Durbin, M. K.; Lin, W. P.; Wong, G. K.; Dutta, P. *Langmuir* **1996**, *12*, 4218−4223.

functionalization approach yields relatively pinhole-free $(SiO_2)_x$-like dielectric layers with the aforementioned characteristics on oxide surfaces with Angstrom-level control over the thickness. Using a well-characterized TPD/Alq heterostructure type, hole-only devices, and cathodes of varying work function, we show that these anode functionalization layers can effect significant modulation of OLED device turn-on voltage as well as external quantum and luminous efficiency. Moreover, we present a theoretical/computational model that accounts for these characteristics and the unusual $(SiO_2)_x$ thickness-dependent aspects of the luminous and current−voltage response.

Experimental Section

Reagents and Physical Measurements. Pentane (Fisher Scientific) and heptane (Fisher Scientific) were distilled from Na/K alloy immediately before use. Octachlorotrisiloxane ($Si_3O_2Cl_8$) was prepared and purified according to the procedure of Schumb.[19] The hole transport material *N*,*N*′-diphenyl-*N*,*N*′-bis(3-methylphenyl)-(1,1′-biphenyl)-4,4′-diamine (TPD) was obtained from Aldrich and gradient-sublimed before use. Tris(8-hydroxyquinolinato)aluminum(III) (Alq, Aldrich) was doubly gradient -sublimed. Tetra-*n*-butylammonium perchlorate (TBAP) was recrystallized from an ethyl acetate/hexane solution and dried under vacuum at 100 °C for 10 h. The deposition of self-assembled dielectric layers was performed under rigorously anhydrous/anaerobic conditions using standard Schlenk techniques.

Specular X-ray reflectivity experiments on coated single-crystal Si(111) substrates were performed at the Naval Research Laboratory X23B beamline at the National Synchrotron Light Source. Details of this experimental procedure and data analysis are reported elsewhere.[16,18] X-ray photoelectron spectroscopic (XPS) measurements were performed using the Al Kα source of a VG ESCALAB MKII photoelectron spectrometer and, more recently, a monochromatized Al Kα source in a Kratos Axis-Ultra photoelectron spectrometer. UPS measurements were made using a He−I (21.2 eV) illumination source (Omicron) on the same Kratos spectrometer. As-received ITO samples (Donnelly Corp.) were Ar^+ sputter-cleaned to reveal low-intensity photoemission (UPS) from the Fermi edge. All other ITO samples were examined as-received, after deposition (vide infra) of the $(SiO_2)_x$ layers. Atomic force microscopy measurements were performed using a Nanoscope III microscope operating in contact force mode. All images were obtained in air with Si_3N_4 cantilevers having pyramidal tips with 70° cone angles and 20−50-nm radii of curvature. Images were verified by scanning the same area several times to ensure reproducibility as well as by scanning different area sizes to examine image consistency. No attempt was made to correct for AFM tip convolution.[20] Cyclic voltammetry was carried out on a Cypress Systems model CySy 2Ra potentiostat employing self-assembly modified ITO substrate working electrodes ($A \sim 0.70$ cm^2) in standard three-electrode electrochemical cells. All potentials were measured and are reported relative to a pseudo-Ag reference electrode and all cyclic voltammetric measurements were recorded at 100 mV/s. The nonaqueous probe solution (1 mM ferrocene in 0.1 M TBAP) was prepared by passing a HPLC-grade benzene/acetonitrile (1:1) solution through an activated basic alumina column immediately before use. Ferrocene was purified by vacuum sublimation.

Preparation of ITO Substrates for OLEDs. ITO-coated glass (20 Ω/sq. Donnelly Corp.; 20−30-Å rms roughness) was cut into 2.54 × 2.54 cm^2 pieces and then cleaned in an ultrasonic 2-propanol bath, followed by acetone, and finally methanol. Substrates were subsequently treated in an oxygen plasma cleaner for 30 s to remove any residual organic contaminants. An SiO_x strip (120 nm) about 1-cm wide was then vapor-deposited onto the cleaned ITO to avoid short-circuiting of the electrodes during device evaluation. The cleaning process described above was repeated after the SiO_x deposition.

Cleaning Procedure for Silicon Substrates. Silicon (111) substrates (Semiconductor Processing Co.) were immersed in "piranha" solution (concentrated H_2SO_4:30% H_2O_2; 70:30 v/v) at 80 °C for 1 h. After cooling to room temperature, substrates were rinsed repeatedly with deionized (DI) water followed by an RCA-type cleaning protocol (H_2O:30%H_2O_2:NH_3; 5:1:1 v/v/v; sonicated at room temperature for 40 min). Substrates were finally rinsed with copious amounts of DI water, heated to 125 °C for 15 min, and dried in vacuo.

Deposition of Self-assembled Siloxane Dielectric Layers. Cleaned ITO or Si(III) substrates were heated in air at 125 °C for 15 min and placed into a Schlenk-type reaction vessel where a vacuum of 25−50 mTorr was applied for 20 min to remove excess surface water; the vessel was then backfilled with nitrogen. A 24.0 mM solution of octachlorotrisiloxane in freshly distilled heptane was added under an inert atmosphere to the reaction vessel in sufficient quantity to totally immerse the substrates. The substrates were allowed to react with the stirring siloxane solution under nitrogen for 30 min. Following removal of the siloxane solution by cannula, the substrates were rinsed and sonicated two successive times in freshly distilled dry pentane under nitrogen. The substrates were then removed from the reaction vessel, washed, sonicated with acetone, and subsequently dried in air at 125 °C for 15 min. This process was repeated to form dielectric layers of incrementally increasing thickness.

Fabrication of OLED Devices. The bare and self-assembly modified ITO substrates were loaded into a bell jar deposition chamber housed in a nitrogen-filled glovebox. At 10^{-5}−10^{-6} Torr, a 60-nm layer of TPD was first deposited, followed by 60 nm of doubly gradient-sublimed Alq. Both organic layers were grown at a deposition rate of 1 Å/s. Following the deposition of the organic layers, a 200-nm-thick Al cathode was deposited through a shadow mask. This metallic layer was patterned to give six devices, each with an area of 0.12 cm^2.[3f] The device output power was measured with a calibrated Si photodiode and was then converted to photons·s^{-1}. The ratio of the photons·s^{-1} to current defines the external quantum efficiency. As presented here, turn-on voltage is defined as the voltage when emitted light is first detected.

Fabrication of Hole-Only Devices. Bare and self-assembly modified ITO substrates were loaded into a bell jar deposition chamber housed within a nitrogen-filled glovebox. At a maximum base pressure of 2×10^{-5} Torr, TPD (2500 Å) was vapor-deposited at a rate of ∼3 Å/s. Following TPD deposition, substrates were sputter-coated with 60 Å of Au through the same shadow mask employed for OLED fabrication described above. Single-carrier device assembly was subsequently completed with the masked thermal vapor deposition (maximum base pressure 2×10^{-5} Torr) of Al (150 nm). Device behavior was evaluated using a computer-controlled Keithley 2400 source meter.

Results

We report here the growth, microstructural characterization, and current/luminous function in organic heterostructures, of thin, contiguous, dielectric films deposited at the anode−organic interface of archetypical vapor-deposited OLEDs. By utilizing the high reactivity of chlorosilyl functionalities toward hydroxylated surfaces,[16,17,21] films having a $(SiO_2)_x$-type microstructure

(19) Schumb, W. C.; Stevens, A. J. *J. Am. Chem. Soc.* **1947**, *69*, 726.

(20) Hulteen, J. C.; Treichel, D. A.; Smith, M. T.; Duval, M. L.; Jensen, T. R.; Van Duyne, R. P. *J. Phys. Chem. B* **1999**, *103*, 3854−3863, and references therein.

(21) Ulman, A. *An Introduction to Ultrathin Organic Films From Langmuir−Blodgett to Self-Assembly*; Academic Press: San Diego, 1991; pp 237−304.

Scheme 1. Procedure for Layer-by-Layer Chemisorptive Self-assembly of $(SiO_2)_x$ Layers upon ITO Surfaces and Their Subsequent Incorporation into OLED Heterostructures[a]

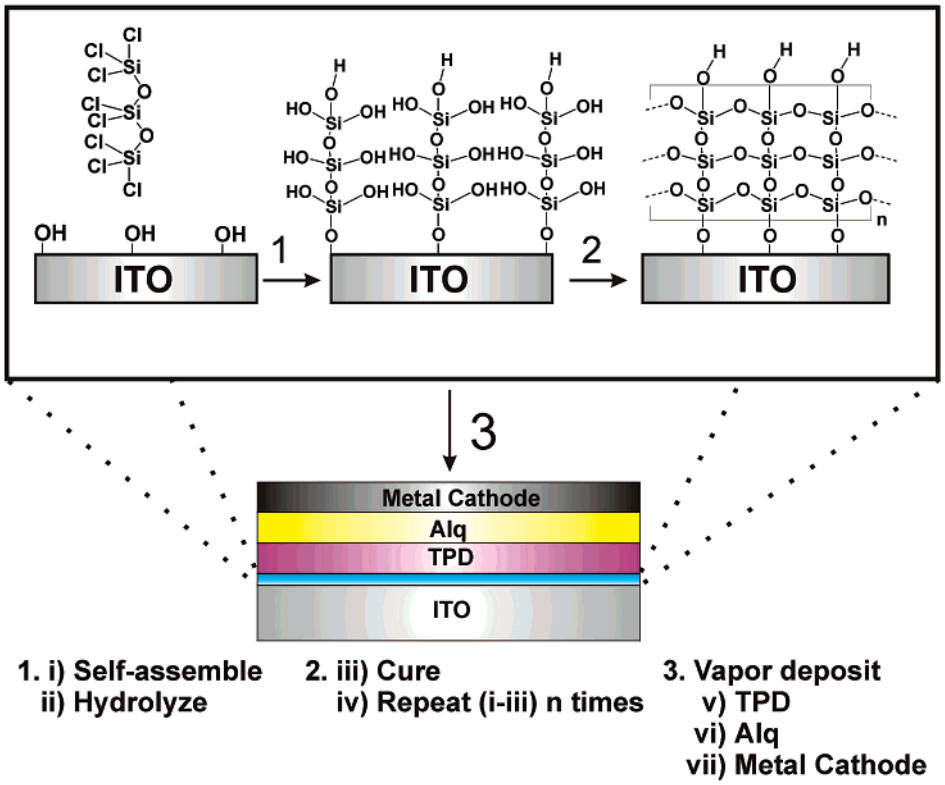

[a] The layer thickness created on each successive $Si_3O_2Cl_8$ deposition is 8.3(1) Å.

can be deposited via a self-limiting, solution-based chemisorption process.[16,22] The growth, microstructure, and electronic properties of these films are first discussed, followed by their influence on OLED characteristics. A theoretical model is presented to explain the $(SiO_2)_x$-thickness dependence of the device response.

Monolayer Synthesis and Self-assembly. As illustrated in Scheme 1, multiple layers of octachlorotrisiloxane can be sequentially chemisorbed from dry hydrocarbon solutions onto clean ITO-coated glass or single-crystal Si(111) surfaces. These surfaces possess hydroxyl functionalities and adsorbed water,[23] which are reactive toward chlorosilyl groups, thereby affording covalent fusion of the siloxane molecule to the surface. Exposure to ambient and subsequent hydrolysis of the film acts to totally convert any unreacted chlorosilyl groups into silanol functionalities. Following thermal curing/cross-linking in air at 125 °C, a thin layer of dielectric material is formed on the ITO surface. The properties of these films are discussed below. Incorporation of these self-assembled $(SiO_2)_x$ films into OLED devices (see Scheme 1) will be shown to significantly affect turn-on characteristics and luminous efficiencies.

Specular X-ray Reflectivity Measurements. Film Thickness, Density, and Interfacial Structure. To determine the thickness and microstructure of the dielectric layers formed with each successive deposition, specular X-ray reflectivity (XRR) measurements were performed upon a series of films deposited on the native oxide surface of single-crystal Si(111), using the self-assembly procedure discussed above. Figure 1a shows the X-ray reflectivity data normalized to the Fresnel reflectivity, for a film formed by four successive chemisorptive $Si_3O_2Cl_8$ depositions. Fitting of these data to a physically reasonable model provides details of the film thickness, smoothness, interfacial abruptness, and density. In general, the reflectivity can be expressed in terms of the average electron density by eqs 1 and 2,[17c,18,24] where R_F is the theoretical Fresnel reflectivity

$$R(k_z) = R_F(k_z)|\Phi(k_z)|^2 \quad (1)$$

$$\Phi(k_z) = \int \frac{1}{\rho_\infty}\frac{d\langle\rho\rangle}{dz} e^{ik_z z}\, dz \quad (2)$$

for a smooth interface, k_z is the momentum transferred ($k_z = 4\pi/\lambda \sin\theta$), $d\langle\rho\rangle/dz$ is the derivative of the electron density along the surface normal direction, averaged over the in-plane coherence length of the X-rays, and ρ_∞ is the electron density of the substrate (Si).

By fitting XRR data as in Figure 1a, it is possible to determine the thickness of the deposited film as well

(22) (a) van der Boom, M. E.; Evmenenko, G.; Dutta, P.; Marks, T. J. *Chem. Mater.* **2001**, *13*, 15−17. (b) Yitzchaik, S.; Marks, T. J. *Acc. Chem. Res.* **1996**, *29*, 197−202. (c) Roscoe, S. B.; Yitzchaik, S.; Kakkar, A. K.; Marks, T. J.; Xu, Z. Y.; Zhang, T. G.; Lin, W. P.; Wong, G. K. *Langmuir* **1996**, *12*, 5338−5349. (d) Parikh, A. N.; Allara, D. L.; Azouz, I. B.; Rondlez, F. *J. Phys. Chem.* **1994**, *98*, 7577−7590.

(23) (a) Milliron, D. J.; Hill, I. G.; Shen, C.; Kahn, A.; Schwartz, J. *J. Appl. Phys.* **2000**, *87*, 572−576. (b) Gardner, T. J.; Frisbie, C. D.; Wrighton, M. S. *J. Am. Chem. Soc.* **1995**, *117*, 6927−6933. (c) Wilson, R.; Schiffrin, D. J. *Analyst* **1995**, *120*, 175−178. (d) Chen, K.; Caldwell, W. B.; Mirkin, C. A. *J. Am. Chem. Soc.* **1993**, *115*, 1193−1194.

(24) Tidswell, I. M.; Ocko, B. M.; Pershan, P. S.; Wasserman, S. R.; Whitesides, G. M.; Axe, J. D. *Phys. Rev. B* **1990**, *41*, 1111−1128.

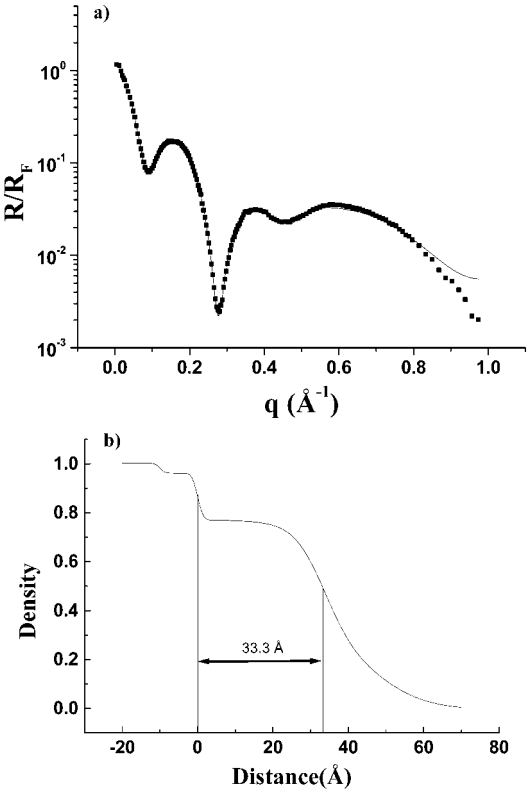

Figure 1. (a) Representative X-ray reflectivity data showing the response from four $(SiO_2)_x$ layers successively self-assembled via the procedure of Scheme 1 on the native oxide surface of single-crystal Si(111). The solid line represents the best fit to the data using a three-layer $Si/SiO_2/(SiO_2)_x$ model. (b) Electron density profile of the above fit. Electron densities have been normalized to the Si substrate. The origin of the *x* axis is at the center of the film−substrate interface.

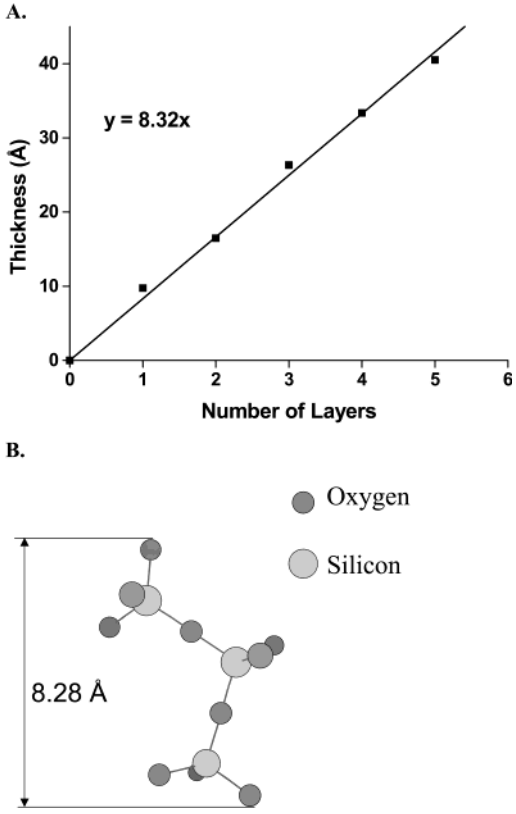

Figure 2. (a) X-ray reflectivity-derived thickness data for self-assembled $(SiO_2)_x$ layers deposited on single-crystal Si(111), showing the monotonic increase in total film thickness with number of depositions. The line is a least-squares fit to the data. (b) Semiempirical AM1 quantum mechanical energy minimized model structure of a model octahydroxytrisiloxane fragment oriented on a surface to illustrate a plausible fit to an 8.3-Å extension. Hydrogen atoms are omitted for clarity of viewing.

as the electron density profile of the $(SiO_2)_x$ layer, as shown in Figure 1b. The electron density−distance profile in Figure 1b reveals that the electron density undergoes an initial decrease as the transition is made from the Si substrate to the native oxide overlayer on the substrate surface. Further from the substrate surface, a second decrease in electron density that corresponds to the native oxide-deposited dielectric film interface is observed. Measurement of the electron density in this region provides a value for the total thickness of the deposited dielectric film, which in the case of Figure 1b is 33.3 Å. Note also that the derived electron density of the deposited $(SiO_2)_x$ layer is ∼85% that of the native oxide, indicating the formation of a relatively dense microstructure.

X-ray reflectivity measurements (Figure 2a) on a series of dielectric-coated Si(111) substrates indicate that the total deposited film thickness increases monotonically with repeated layer depositions. From the slope of the least-squares line, it can be inferred that each exposure to the $Si_3O_2Cl_8$ solution results in deposition of a 8.3 ± 0.1 Å thick $(SiO_2)_x$ layer. This individual layer thickness can be convincingly modeled by a surface-anchored octahydroxytrisiloxane molecule (Figure 2b) using AM1-level semiempirical energy minimization performed with the program CS Chem3D Pro (CambridgeSoft Corp.). Here, a calculated dimension of ∼8.28 Å is estimated for a single molecule, although the actual layer internal connectivity is doubtless more complex. This linearity in the $(SiO_2)_x$ deposition process affords considerable precision in tailoring the cumulative dielectric thickness.

Atomic Force Microscopy Studies. Film Morphology. AFM imaging of a four-layer self-assembled dielectric film deposited on single-crystal Si(111) (Figure S1; Supporting Information) indicates the $(SiO_2)_x$ film is essentially featureless and extremely smooth, with no indication of island growth, film cracking, or pitting. It is indistinguishable from the Si(111) substrate image, and the apparent estimated rms roughness is ≤2.0 Å. This argues that the present self-assembly process is capable of depositing dielectric films as smooth, uniform, continuous layers.

X-ray Photoelectron Spectroscopy. Surface Coverage and Composition. Figure 3 presents a series of XPS spectra for an unmodified, clean, bare ITO surface and similar ITO surfaces covered successively with one, two, and four layers of self-assembled siloxane dielectric. There is a marked decrease in both the In(3d) and Sn(3d) features as the dielectric layer coverage increases, which is accompanied by a corresponding increase in both the Si(2p) and Si(2s) intensities, and, most importantly, a monotonic increase in the Si(2p)/In(3d) intensity ratio, as expected for layer-by-layer growth.[14,16−18,25] Upon deposition of a single $(SiO_2)_x$

(25) Lüth, H. *Surfaces and Interfaces of Solids*; Springer-Verlag: New York, 1993; Vol. 15, pp 101−114.

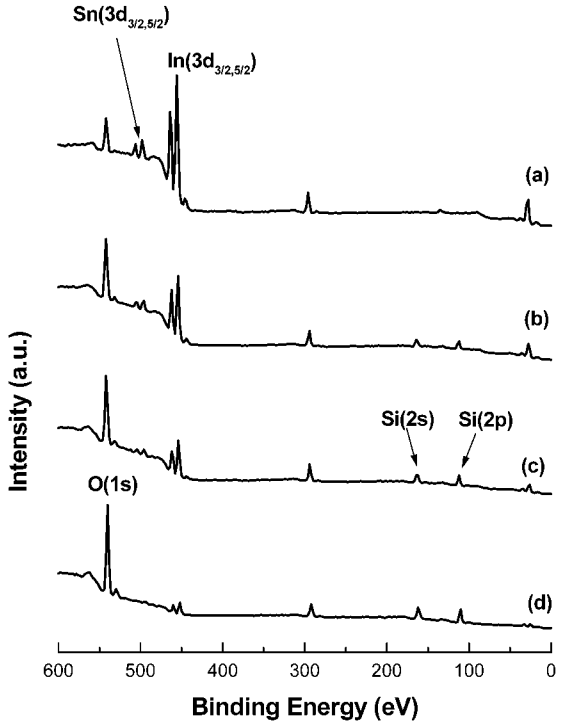

Figure 3. XPS spectra (Al Kα excitation) of (a) bare ITO, (b) one layer, (c) two layers, and (d) four layers of self-assembled $(SiO_2)_x$ film.

layer, the In(3d) intensity decreases by ∼50% with respect to that of the bare surface, as anticipated for a conformal, approximately pinhole-free film, where the emitted photoelectrons have a kinetic energy of ∼1000 eV (Al Kα excitation), hence, an inelastic mean free path of ∼30 Å. Under these conditions, the intensity is expected to decrease exponentially with each added monolayer.[26] Furthermore, the Cl(2p) photoemission peaks are just at the detection limit for this spectroscopy, indicating at most approximately part-per-thousand chloride concentration in the near-surface region, consistent with full hydrolysis of the Si−Cl bonds during the self-assembly process as depicted in Scheme 1. Likewise, these results indicate that negligible quantities of In chlorides are formed in the self-assembly/hydrolysis/cure process. The O(1s) signal arises from both the ITO substrate and the deposited dielectric and is therefore not used in this characterization. The C(1s) signal on the as-received ITO is of nearly the same magnitude as the SAM-modified ITO surfaces and is judged to be due to adventitious carbon and not to be an indicator of the dielectric film surface coverage.

Ultraviolet Photoelectron Spectroscopy. Work Function. UPS measurements were conducted on clean (as-received) ITO, ITO that had been Ar^+-sputtered in vacuo to remove the last vestiges of carbon, and on ITO surfaces covered with one to four monolayers of the dielectric material. Estimates of the effective surface work function can be obtained from the measured width of the UV−photoemission spectrum, subtracted from the source energy,[27,28] using the high and low kinetic energy edges of the photoemission spectrum for this measurement. In the present study, the sputter-cleaned ITO surface exhibits a spectral width of 16.2−16.4 eV, indicating a surface work function of 4.9 ± 0.1 eV, which is within the relatively wide range of work functions reported for ITO.[23a,29] For the $Si_3O_2Cl_8$-modified ITO surfaces, the width of the photoemission spectra decreases to ca. 14.0 ± 0.2 eV, yielding an estimated surface work function for all samples of 7.1 ± 0.2 eV (layer thickness, Φ: 8 Å, 7.2 eV; 17 Å, 7.5 eV; 25 Å, 6.9 eV; 33 Å, 7.1 eV). This shift in the apparent work function is accompanied by a shift in the low kinetic energy edge of the photoemission spectrum by only ∼0.1−0.3 eV, indicating a minor shift in the vacuum level due to the formation of interface dipoles.[27,28] The present UPS data are therefore consistent with essentially complete coverage of the ITO surface with insulating dielectric layers (the UPS penetration depth is ∼5−20 Å)[26] and that the bulk of the change in effective work function arises from the offset in energy between the ITO Fermi edge and the upper edge of the dielectric HOMO level. The net effect of this modification is to lower the ITO surface Fermi level from ∼0.3 eV above the TPD HOMO level (I ∼ 5.2. eV)[27,30] to as much as ∼1.5−1.8 eV below it.

Cyclic Voltammetry. Film Pinhole Assay. A series of cyclic voltammograms for the oxidation/reduction of a 1.0 mM ferrocene solution in acetonitrile, using a clean, bare ITO surface and a series of modified ITO surfaces covered with one, two, three, and four layers of the self-assembled $(SiO_2)_x$ material as the working electrode (Figure 4A). As judged both by the separation between anodic and cathodic peaks, and by the overall magnitude of current flowing at any potential, there is a successive passivation of the ITO surface with respect to this redox chemistry as the dielectric layer thickness is successively increased. This process is dependent upon the type of solvent and redox probe molecule employed. Thus, in aqueous media with complete ITO surface coverage by the dielectric layer, it is also possible to suppress significantly the reduction/oxidation processes for a 1.0 mM ferricyanide solution with only one to two layers of the dielectric material (Figure 4B). Electrochemical responses of other passivated electrode surfaces possessing pinhole densities of <1% of the geometric area lead to current/voltage responses similar to those in Figure 4.[31] This suggests that three to four layers of the self-assembled dielectric layer are sufficient to eliminate the majority of pinholes, which would compromise OLED device performance.

Anode Modification Effects on Organic Light-Emitting Diode Response. Conventional OLED devices consisting of a TPD hole transport layer and an Alq electron transport/emissive layer (TPD and Alq were rigorously purified) were fabricated via vacuum deposition onto bare and self-assembly modified glass/ITO

(26) Seah, M. P. In *Practical Surface Analysis by Auger and X-ray Photoelectron Spectroscopy*; Briggs, D., Seah, M. P., Eds.; John Wiley and Sons, Ltd.: New York, 1983; Vol. 14, pp 181−216.

(27) Ishii, H.; Sugiyama, K.; Ito, E.; Seki, K. *Adv. Mater.* **1999**, *11*, 605−625, and references therein.

(28) (a) Schlaf, R.; Parkinson, B. A.; Lee, P. A.; Nebesny, K. W.; Jabbour, G.; Kippelen, B.; Peyghambarian, N.; Armstrong, N. R. *J. Appl. Phys.* **1998**, *84*, 6729−6736. (a) Schlaf, R.; Parkinson, B. A.; Lee, P. A.; Nebesny, K. W. *J. Phys. Chem. B* **1999**, *103*, 2984−2992.

(29) Kim, J. S.; Lagel, B.; Moons, E.; Johansson, N.; Baikie, I. D.; Salaneck, W. R.; Friend, R. H.; Cacialli, F. *Synth. Met.* **2000**, *111*, 311−314.

(30) From UPS measurement of a thin film deposited on Au: Lee, P. A.; Armstrong, N. R.; Chou, H.; Marks, T. J., unpublished results.

(31) Finklea, H. In *Electroanalytical Chemistry*; Bard, A. J., Rubenstein, I., Eds.; Marcel Dekker: New York, 1996; Vol. 19, pp 177−194.

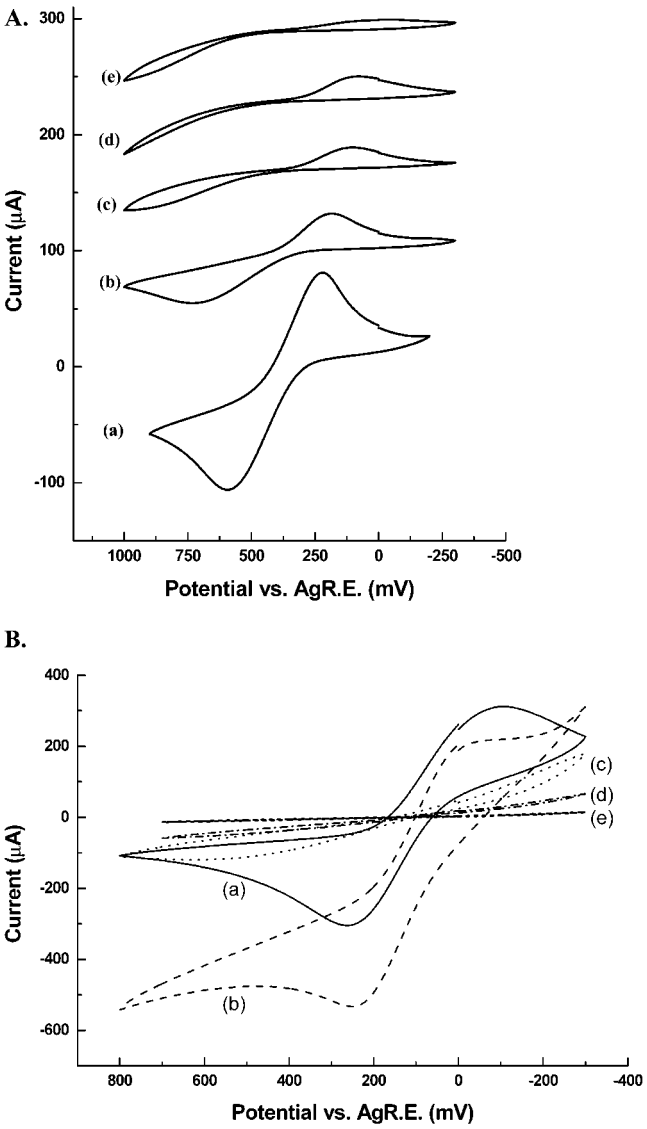

Figure 4. (A) Cyclic voltammetry of a 1.0 mM ferrocene solution at (a) a bare ITO-on-glass surface and with (b) one layer, (c) two layers, (d) three layers, and (e) four layers of self-assembled $(SiO_2)_x$ overlayer deposited on ITO-coated glass. (B) Cyclic voltammetry of a 2.0 mM aqueous $K_3Fe(CN)_6$ solution in a 0.1 M KCl electrolyte at (a) a bare ITO-on-glass surface and with (b) one layer, (c) two layers, (d) three layers, and (e) four layers of self-assembled $(SiO_2)_x$ overlayer deposited on ITO-coated glass. The sweep rate in both sets of experiments is 100 mV/s and the electrode area is ~0.7 cm^2.

anodes. Without exposure to ambient, vapor deposition of a metal cathode completed fabrication of a series of devices having the following structure: ITO/SA dielectric layer (8−33 Å)/TPD (600 Å)/Alq (600 Å)/metal cathode (2000 Å). Figure 5 shows current density and log(forward light output) as a function of bias voltage for a series of devices with Al cathodes and varying thicknesses of self-assembled dielectric layers deposited on the ITO anode. Note that incorporation of the first dielectric layer at the ITO−TPD interface results in a significant increase in the device turn-on voltage (defined here as the point where the luminence reaches 50 cd/m^2). As will be seen, this effect likely reflects, among other factors, the added barrier to hole injection that would be introduced by the incorporation of a thin insulating layer at the ITO−organic interface. As is

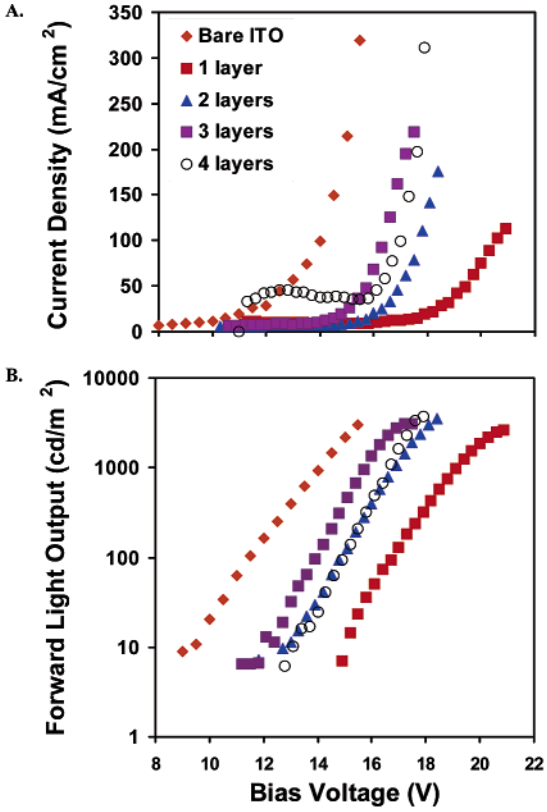

Figure 5. Current density (A) and log-forward light output (B) vs bias voltage plots for ITO/$(SiO_2)_x$/TPD(600 Å)/Alq(600 Å)/Al (2000 Å) OLEDs, showing the effect of interposing self-assembled $(SiO_2)_x$ layers at the anode−hole transport layer interface. The lines through the data points are drawn as a guide to the eye.

evident in Figures 5A,B while incorporation of a single 8.3-Å layer of dielectric film results in a large increase in turn-on voltage, *subsequent incremental increases in $(SiO_2)_x$ thickness by 8.3 and 16.6 Å lead to successively lower turn-on voltages (more current flow and light output for a given voltage).* Interestingly, incorporation of four dielectric layers at the anode−HTL interface reverses this trend and the turn-on voltage again *increases*, presumably reflecting increasing barrier height with insulating film thickness. All OLEDs fabricated with the self-assembled dielectric films invariably exhibit higher forward light output than bare ITO devices at all current densities (Figure S2, see Supporting Information). This behavior is also evident in Figure 6, which shows forward external quantum (photons out/electrons in) and luminous efficiencies (lm/W) as a function of $(SiO_2)_x$ thickness. Note that incorporation of a single, ~8.3-Å-thick self-assembled dielectric layer has the effect of more than doubling maximum device quantum efficiency.

To isolate the hole injection characteristics of the dielectric-functionalized anodes, "hole-only" devices[32] of structure ITO/$(SiO_2)_x$/TPD(2500 Å)/Au(60 Å)/Al(2000 Å) were fabricated and characterized. Current density versus applied bias and log(current density) versus log(electric field) are shown in Figure 7.[33] It can be

(32) Giebeler, C.; Antoniadis, H.; Bradley, D. C.; Shirota, Y. *J. Appl. Phys.* **1999**, *85*, 608−615, and references therein.
(33) Arkhipov, V. I.; Emelianova, E. V.; Tak, Y. H.; Bässler, H. *J. Appl. Phys.* **1998**, *84*, 848−856.

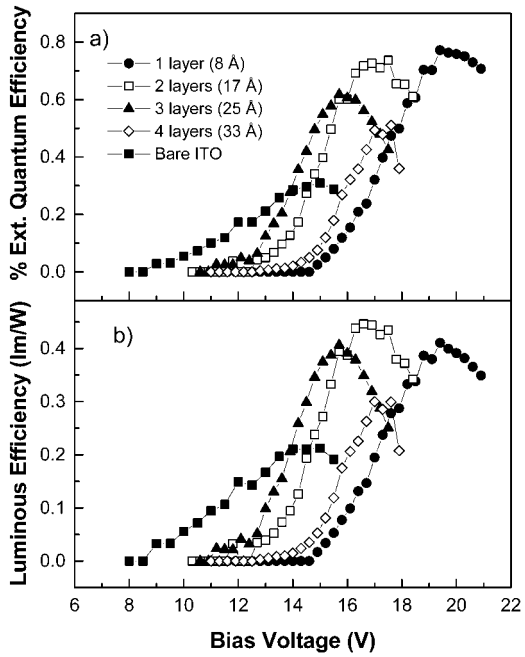

Figure 6. Forward external quantum efficiency (a) and luminous efficiency (b) vs voltage plots for ITO/$(SiO_2)_x$/TPD(600 Å)/Alq(600 Å)/Al (2000 Å) OLEDs, showing the effect of incorporating various numbers of self-assembled dielectric layers at the anode−hole transport layer interface. The lines through the data points are drawn as a guide to the eye.

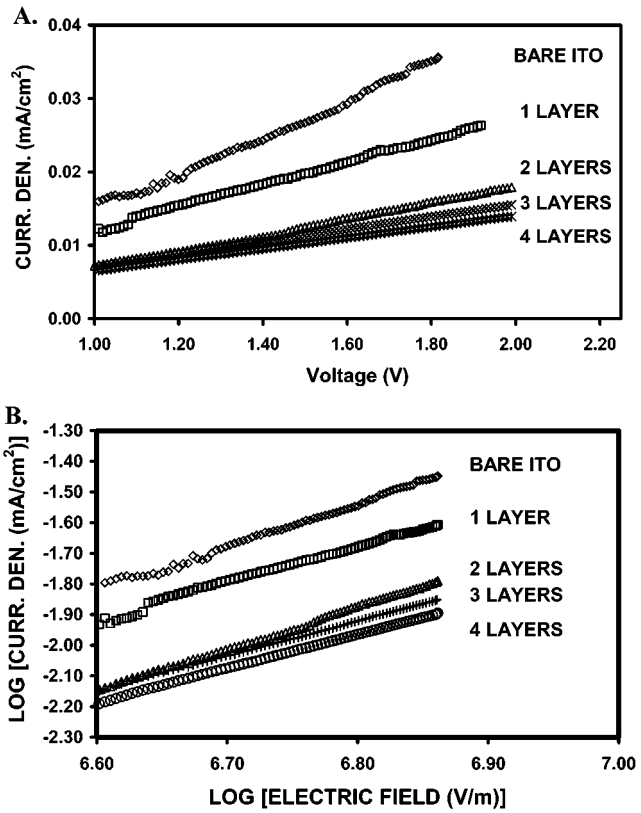

Figure 7. "Hole-only device" data for a series of ITO/$(SiO_2)_x$/TPD(2500 Å)/Au(60 Å/Al(2000 Å) heterostructures as a function of $(SiO_2)_x$ thickness, plotted as current density versus voltage (A) and log(current density) versus log(electric field) (B).

clearly seen that the effect of incrementally increasing the dielectric layer thickness is to incrementally suppress hole injection from the ITO anode into the TPD hole transport layer. Interestingly, the effect of layer

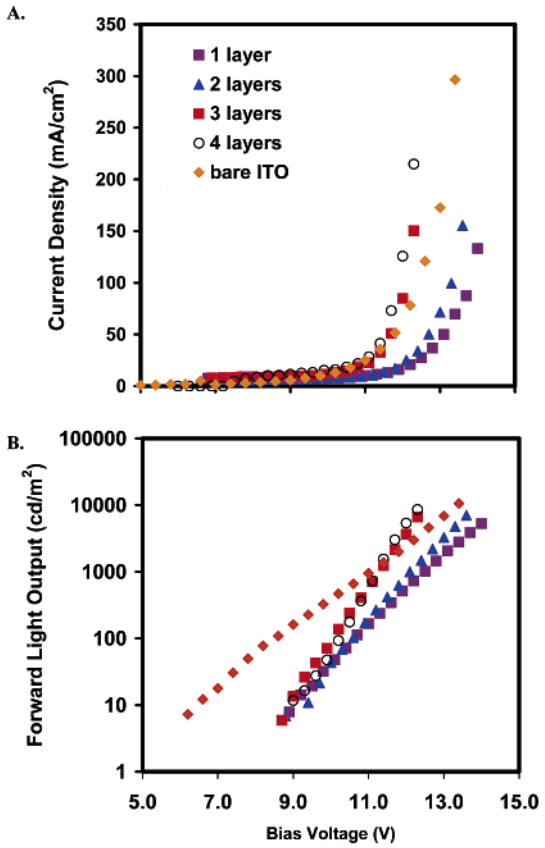

Figure 8. Current density vs (A) log-forward light output (B) voltage plots for ITO/$(SiO_2)_x$/TPD(600 Å)/Alq(600 Å)/Mg (2000 Å) OLEDs, showing the effect of incorporating various numbers of self-assembled dielectric layers at the anode−hole transport layer interface. The lines through the data points are drawn as a guide to the eye.

thickness is not monotonic, but rather the greatest diminution of hole injection occurs upon application of the first and second 8.3-Å dielectric layers.

Alterations in the cathode−ETL interface or in the cathode material can also be employed as OLED mechanistic probes because they can alter the hole−electron injection balance by altering the work function, hence, the barrier to electron injection. A priori, using a Mg cathode instead of Al should enhance electron injection efficiency as a consequence of the improved energetic match between the Mg work function (3.7 vs 4.3 eV for Al) and the Alq LUMO level (3.1 eV).[34] Current density and log-forward light output versus voltage plots are shown in Figure 8 for OLED devices differing in structure from those in Figure 5 only in the cathode material. As can be seen in Figure 8, incorporation of the self-assembled $(SiO_2)_x$ layers at the anode−organic interface has diminished effects; however, the same qualitiative trend remains: incorporation of a single, 8.3-Å dielectric layer greatly increases the operating voltage, while devices with subsequent thicker layers operate at lower voltages with the $(SiO_2)_4$ device again shifting to higher operating voltage. Forward light output versus current density plots for these Mg-based devices (Figure 2S, see Supporting Information) reveal that incorporation of the self-assembled $(SiO_2)_x$ layers into the Mg device has a smaller affect on device

(34) Kalinowski, J.; DiMarco, P.; Cocchi, M.; Fattori, V.; Camaioni, N.; Duff, J. *Appl. Phys. Lett.* **1996**, *68*, 2317−2319.

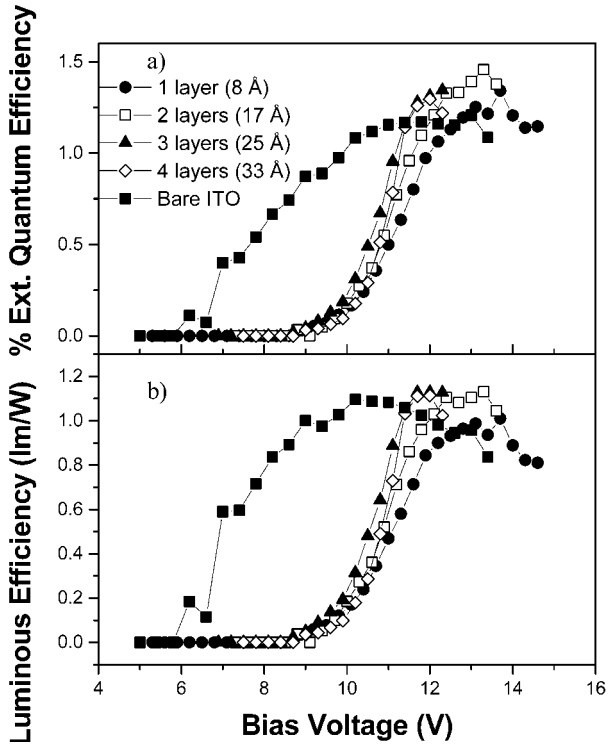

Figure 9. External quantum efficiency (a) and luminous efficiency (b) vs voltage plots for ITO/$(SiO_2)_x$/TPD(600 Å)/Alq(600 Å)/Mg (2000 Å) OLEDs, showing the effect of incorporating various numbers of self-assembled dielectric $(SiO_2)_x$ layers at the anode−hole transport layer interface. The lines through the data points are drawn as a guide to the eye.

performance than in the corresponding Al devices. Furthermore, the forward external quantum and luminous efficiency plots presented in Figure 9 reveal a compressed but qualitatively similar response due to anode functionalization versus the Al-based devices of Figure 6. The generally lower operating voltages and higher external quantum and luminous efficiencies in the Mg devices versus Al reflect the lower barrier to electron injection and more productive use of the injected holes.[2,3]

Discussion

Anode Functionalization. Microstructure-Charge Injection-Luminence Effects. On the basis of several complementary lines of physicochemical characterization, the present experimental results indicate that self-assembly of insulating $(SiO_2)_x$ structures via layer-by-layer, self-limiting siloxane chemisorption affords smooth, conformal, relatively dense, microstructurally/electronically well-defined layers with sub-nanometer control over total layer thickness. XRR measurements on a single-crystal model substrate indicate a constant thickness is added with each repetition of the deposition sequence in Scheme 1. AFM reveals the deposition of smooth and conformal films with no evidence of pinholes or cracking. The lack of widespread pinholes is further supported by electrochemical studies on coated ITO substrates, which reveal electrode passivation by the self-assembled $(SiO_2)_x$ layers. XPS data additionally verify that the $Si_3O_2Cl_8$ precursor undergoes rapid and complete chemisorptive hydrolysis, thus creating a contiguous $(SiO_2)_x$ film that completely covers the ITO surface as evidenced by the paucity of Cl photoelectrons. The UPS data are also consistent with complete coverage of the ITO surface and reveal a significant positive shift in the ITO surface work function, which is, within the detection limits, insensitive to the $(SiO_2)_x$ layer thickness. The present study arguably yields structurally the most complete picture to date of an OLED anode functionalization process—a requisite for understanding and modeling device response.

As noted in the discussion of OLED device response (vide supra), the striking aspects of ITO/$(SiO_2)_x$/TPD/Alq/Al and ITO/$(SiO_2)_x$/TPD/Alq/Mg heterostructure characteristics as a function of x are as follows: (i) increased ITO work function with dielectric functionalization, (ii) increased quantum efficiency and turn-on voltage with interposition of an 8-Å interfacial dielectric layer at the anode−HTL interface, (iii) slightly declining quantum efficiency and decreasing turn-on voltage (more current and light for a given bias) with further, incremental increases in dielectric layer thickness to ∼25 Å, (iv) decreased quantum efficiency and increased turn-on voltage when the dielectric thickness reaches ∼33 Å, (v) nonmonotonic decrease in injected hole fluence with incremental increases in dielectric layer thickness, and (vi) qualitatively similar but compressed heterostructure response for Mg versus Al cathodes, with voltage features shifted to lower bias. At an initial, broad level of analysis, certainly the better work function−ETL LUMO energetic match of Mg/Alq versus Al/Alq accounts for the generally lower turn-on characteristics of the Mg cathode system. That quantum efficiency is enhanced by the interfacial anode−HTL dielectric layer is consistent with other evidence that TPD/Alq devices are, especially with Al cathodes, electron flux-deficient[2] so that any barrier to/attenuation of[13f,15b,c] hole injection should, a priori, afford better balance with electron injection, hence, more productive (and less destructive[35]) use of holes. Such an effect would result in increased quantum efficiency. However, this qualitative picture cannot explain many details of features (i)−(vi) outlined above.

The present observed increase in heterostructure quantum efficiency with anode dielectric functionalization is in partial phenomenological agreement with two other recent studies in which the microstructure and contiguity of dielectric structures, grown by *nonconformal line-of-sight physical vapor deposition techniques* were not as well-characterized. For SiO_2,[13d] $V_{turn-on}$ was found to first fall and then rise with apparent increasing dielectric thickness, while for Al_2O_3,[15b,c] $V_{turn-on}$ rises continuously with apparent increasing dielectric thickness. In both cases, the rationalization for this behavior has been better balance between hole and electron injection into the HTL and ETL, respectively. In direct contrast to this viewpoint, several studies that focused on oxidative treatment of the ITO surface[23a] or chemisorption of molecular dipoles[13c] argued that increasing the effective ITO work function drops the ITO surface Fermi level to an energy closer to or below that of the HTL HOMO, hence, decreasing the intrinsic barrier to hole injection, thus lowering $V_{turn-on}$ and increasing quantum efficiency.

In the present study, it has been possible to insert microstructurally and electrically well-defined dielectric

(35) Aziz, H.; Popovic, Z. D.; Hu, N. X.; Hor, A. M.; Xu, G. *Science* **1999**, *283*, 1900−1902.

layers at the ITO−HTL interface with sub-nanometer thickness control and that, among other effects, these layers substantially increase the anode work function. These results and the OLED current−voltage and luminous response data as a function of anode material and dielectric layer thickness are only partially consistent with mechanisms in which either hole injection is attenuated by the $(SiO_2)_x$ structures, affording better balance of the hole−electron injection fluence, or that the increased ITO work function reduces the barrier to hole injection into the triarylamine HTL. Although both effects may be operative to some degree at appropriate dielectric layer thicknesses with appropriate cathodes, neither alone nor in combination do they explain the present nonintuitive increase and then fall of device operating voltage with increasing layer thickness while the quantum efficiency abruptly increases and then slowly falls. In the following section, we propose a model to explain this additional complexity.

Theoretical Model of Enhanced "Built-In" Field. We propose that the qualitatively new behavior observed here in OLED response with increasing $(SiO_2)_x$ thickness arises from structural and electronic specifics of the self-assembly process. Understanding these effects is significant because a potential opportunity exists to control and improve OLED performance. It is suggested that the incorporation of even a single $(SiO_2)_x$ monolayer strongly suppresses hole injection compared to bare ITO; this is supported by the hole-only device results (Figure 7) and is different from the straightforward expectation following a change in the work function. The present UPS measurements suggest that the effective Fermi energy of ITO with a self-assembled surface monolayer drops below the TPD HOMO level; this would formally lead to charge redistribution, fixing the ITO Fermi level below the top of the HOMO of TPD. However, any charge transferred into the TPD layer at zero bias voltage will be trapped in the image potential,[36] and the image potential barrier can be larger than the hole injection barrier for the bare ITO. In fact, this energy barrier can reach the 1-eV scale,[8,37] while the present intrinsic hole injection barrier is only ∼0.3 eV for ITO. In addition, energy disordering can contribute an additional trapping energy for this transferred charge.[38] Therefore, an increase in the ITO work function could, in principle, lead to strong diminution of the hole injection efficiency.

The present OLED response measurements show (Figure 5) that further increase of the $(SiO_2)_x$ layer thickness leads, for a given bias, to increasing current flow through the heterostructure (the response of the $(SiO_2)_4$ systems is somewhat more complex; see below) and a decrease in the turn-on voltage by ∼2−4 V. To explain this behavior, two alternative models can be considered:

(A) Incorporation of the dielectric layers suppresses hole injection to such an extent that the electrons become the majority carriers. The increase of siloxane layer thickness (up to the limit at which the charges become balanced) then must lead to increased electron injection efficiency.

(B) Further increases in dielectric layer thickness increase the efficiency of hole injection, with the holes remaining the majority carriers.

Regarding mechanism A, if we assume that introduction of the dielectric layers alters the majority carriers, then a qualitative understanding of the observed behavior can be based on a built-in voltage within the self-assembled layer. The built-in voltage can be modeled by a voltage drop across the $(SiO_2)_x$ layer caused by alternating charged planes (negatively charged oxide layers, positively charged Si or H layers; Figure 10) and the large separation between the upper positively charged H layer and the negatively charged anode surface. An increase in the self-assembled layer thickness leads to an increase in this built-in voltage while hole injection is attenuated with the increasing number of $(SiO_2)_x$ monolayers as supported by the hole-only device data (Figure 7).

To explain the further decrease in the turn-on voltage with increasing $(SiO_2)_x$ thickness, we suggest that even a single dielectric layer suppresses the injection of holes to such an extent that electron injection becomes more efficient. In other words, the majority carriers are electrons in devices having even one self-assembled siloxane layer chemisorbed on the anode. However, the increase in built-in voltage V_B in the $(SiO_2)_x$ layer leads to an increase of the effective voltage across the active organic material at fixed bias voltage U. The effective

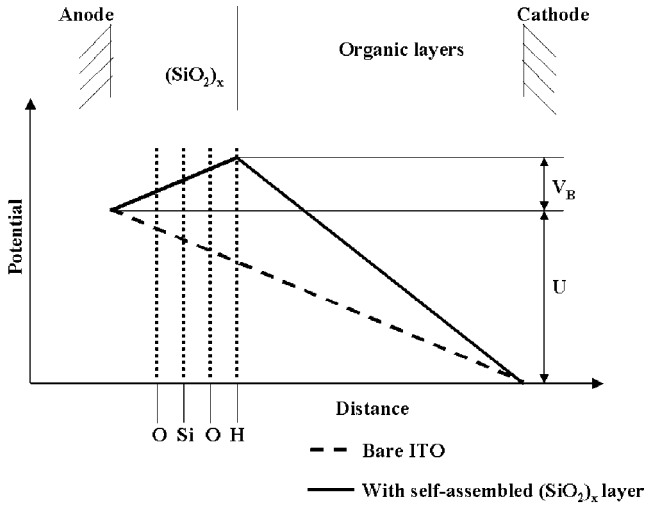

Figure 10. Qualitative model for modification of OLED bias electric field by interposing nanoscopic self-assembled dielectric layers at the anode−hole transport layer interface. The dashed line represents the potential in the absence of the $(SiO_2)_x$ layers and the solid line the change due to $(SiO_2)_x$ incorporation. V_B and U are, respectively, the built-in voltage due to the self-assembled siloxane layers and the applied potential.

(36) (a) Shen, Y.; Klein, M. W.; Jacobs, D. B.; Scott, J. C.; Malliaras, G. G. *Phys. Rev. Lett.* **2001**, *86*, 3867−3870. (b) Klein, M. W.; Dunlap, D. H.; Malliaras, G. G. *Phys. Rev. B* **2001**, *64*, 5332−5346. We thank Prof. Malliaras for a preprint. (c) Bussac, M. N.; Michoud, D.; Zuppiroli, L. *Phys. Rev. Lett.* **1998**, *81*, 1678−1682.

(37) (a) Burin, A. L.; Ratner, M. A. *J. Chem. Phys.* **2000**, *113*, 3941−3944. (b) Wolf, U.; Bässler, H. *Appl. Phys. Lett.* **1999**, *74*, 3848−3850.

(38) The combination of a very large built-in voltage leading to a large elctronic current flow at low voltages and strong suppression of hole tunneling through the thick interface could lead to a large concentration of noncompensated electrons within the layers that would block electron injection, leading to a space charge limited current, weakly dependent on bias voltage. At sufficiently high voltage, additional charge injection mechanisms could enhance hole injection (e.g., electron density accumulation at the PTD−$(SiO_2)_x$ interface). Such processes will be very sensitive to interfacial structural heterogeneities,[37] the modeling of which is currently beyond the scope of the present description.

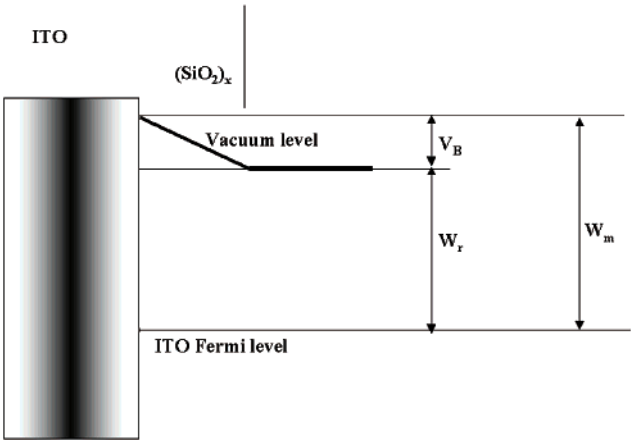

Figure 11. Diagram showing the difference between real (W_r) and measured (W_m) ITO work functions for an OLED anode functionalized with self-assembled $(SiO_2)_x$ layers.

voltage causing electron injection is given by the sum $U + V_B$ (Figure 10). An increase of V_B thus renders electron injection more efficient, and accordingly the turn-on voltage decreases with increasing layer thickness.

This explanation does not contradict the aforementioned UPS results showing that the ITO work function remains nearly unchanged with the increase in $(SiO_2)_x$ thickness. To escape from the ITO, electrons must overcome the contact barrier W_m (Figure 11) that can deviate from the actual energy difference from the vacuum level, W_r, because of the voltage V_B built into the $(SiO_2)_x$ layer. This qualitative model can also be used to interpret the observed effects on quantum efficiency, which is defined by the ratio of emitted photons N_{ph} to injected electrons and holes (N_e and N_h, respectively; eq 3). If holes are majority carriers, then $N_e \ll N_h$, and if electrons are majority carriers, $N_h \ll N_e$. Under conditions of maximum efficiency, all minority carriers

$$Q \propto \frac{N_{ph}}{N_e + N_h} \tag{3}$$

recombine with the majority carriers, and the maximum recombination efficiency is given by eq 4. Thus, the smaller the difference between the numbers of injected electrons and holes, the greater the device efficiency.

$$Q_{max} \propto \frac{\min(N_e, N_h)}{N_h + N_e} \tag{4}$$

For the bare ITO anode, the holes are majority carriers and the maximum recombination efficiency is given by $Q_0 \sim N_e/N_h$. When the first $(SiO_2)_x$ layer is introduced, electrons become majority carriers and the efficiency becomes $Q_1 \sim N_h/N_e$. The observed relationship $Q_1 \sim 3Q_0$ may reflect the resulting changes in the energetics of the surface layer, which is difficult to address quantitatively. Further increases of the $(SiO_2)_x$ layer thickness further suppress the hole injection and enhance the electron injection. This will lead to a decrease of the maximum efficiency given by eq 4, for $x > 1$, in agreement with the data of Figure 6. The $x = 4$ devices additionally exhibit somewhat higher current at lower voltages for both Al and Mg cathodes. This additional complexity may represent an interplay of maximized electronic current and minimized hole injection, the exact treatment of which requires additional structural homogeneity information.[38]

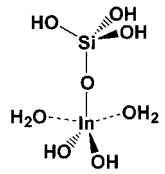

Figure 12. Five-coordinate In^{3+} local model used to compute the change in work function using ab initio electronic structure methods.

Note that the present discussion ignores the effect of the volume charge within the dielectric layers. This charge improves the balance between the carriers because of electroneutrality requirements.[39] The balance effect is less important for the Al-based devices, where charge density is limited by the weak electron injection caused by the high injection barrier at the Al/Alq_3 interface. In contrast, for Mg-based devices, this effect is expected to be much weaker given the substantially increased electron density relative to the Al-based system. Therefore, the present theoretical considerations are primarily suitable for OLEDs where a strong charge volume effect is observed.

An overall reduction of the turn-on voltage with increasing layer thickness by $\Delta V_{turn-on} \sim 2$ V (Figure 5A) requires the same scale for the built-in voltage in the $(SiO_2)_x$ layer. This estimate exceeds the standard scale of the interlayer voltage, which is normally less than ~1 V.[13c] We suggest that this difference reflects the covalent bonding within the siloxane layer, which can constrain the molecular dipole moments to similar orientations, while the usual van der Waals interactions cannot compete with the electrostatic energy of the dipole−dipole interactions that can reduce order in the films.

To examine the consistency of the proposed built-in voltage $V_B \sim 2$ V, a first-principles electronic structure study was carried out on a simple model for the fragment of a self-assembled layer, formed by *n*-coordinate In^{3+} (in the ITO crystal structure $n = 6$[40]) coupled through a single bridging oxygen atom to a tetrahedral SiO_3 center. Hydrogen atoms were used to saturate all In−O− bonds. Geometry optimizations of various structures having six-coordinate In^{3+} lead to expulsion of one water molecule from the coordination sphere. Therefore, we studied a model five-coordinate In^{3+} (Figure 12) structure, which is stable. The value of interest is the dipole moment of this type of fragment. Considering a layer of parallel dipoles, the total voltage drop through such a layer is given by eq 5, where *d* is the dipole

$$V_B = \frac{d}{\epsilon\epsilon_0 A} \tag{5}$$

moment, *A* is the area per single dipole, ϵ is the material dielectric constant, and ϵ_0 is the vacuum dielectric constant. A Hartree−Fock study using the program

(39) (a) Khramtchenkov, D. V.; Arkhipov, V. I.; Bässler, H. *J. Appl. Phys.* **1997**, *81*, 6954−6962. (b) Khramtchenkov, D. V.; Arkhipov, V. I.; Bässler, H. *J. App. Phys.* **1996**, *79*, 9283−9290.

(40) (a) Thilakan, P.; Minarini, C.; Loreti, S.; Terzini, E. *Thin Solid Films* **2001**, *34*, 388, 34−40. (b) Yin, L. T.; Chou, J. C.; Chung, W. Y.; Sun, T. P.; Hsiung, S. K. *Mater. Chem. Phys.* **2001**, *70*, 12−16.

Q-Chem 2.0[41] with the CBKJC basis set and full geometry optimization from various initial configurations leads to an estimate of $d \sim 3.5$ D. The area per single dipole can be estimated by assuming that the dipoles form a square lattice with period given by the distance between two oxygen atoms in the plane parallel to the anode−siloxane interface, 4.2 Å. We then estimate $A \sim 18$ Å^2. Using this parameter and the vapor-deposited SiO_2 dielectric constant $\epsilon = 4$ established previously for thin SiO_2 films,[42] we obtain a voltage drop $V_B \approx 2$ V, which suffices to understand the experimental data. Note that the above results are admittedly (and pragmatically) approximate. Extensive studies on larger fragments would be required to compute a more realistic representation of the experimental data.

Alternative explanation B assumes that holes remain the majority carriers for all $(SiO_2)_x$ thicknesses. The bottleneck then in charge current is hole injection from the traps (arising from the image potential). At a fixed voltage drop (defined by the energetic difference between the modified ITO−siloxane work function and the TPD HOMO level) a reduction of charge injected into the TPD layer is observed with increasing interlayer thickness. In fact, the voltage drop inside the $(SiO_2)_x$ layer is proportional to the product of the charge density and the layer thickness. Therefore, the charge density decreases inversely in proportion to the thickness. The increase of the layer thickness thus should reduce the effective image potential[36] and, correspondingly, the hole injection barrier into the bulk TPD for holes trapped near the siloxane surface. This would also lead to the observed decrease in the turn-on voltage. The observed behavior of quantum efficiency can be explained by the arguments identical to the previous case with the replacement of electrons by holes.

In principle, mechanisms A and B can be distinguished by analysis of the hole-only device data where electronic transport can be neglected because of the large electron injection barrier. If the explanation based on the built-in voltage and majority carrier replacement is correct, then the current should decrease with increasing thickness of the self-assembled layer. Otherwise, the current should first decrease when the single monolayer is inserted and then subsequently increase. To resolve this question, hole-only devices were studied as described above. The measurements (Figure 7) indicate that the hole current density decreases incrementally with increasing dielectric layer thickness.[43] Accordingly, the hole injection barrier increases, presumably because of the increase in the built-in voltage. Hence, the observed increases in measured current density for OLEDs having $x > 1$ versus the single-layer device ($x = 1$; Figure 5a) can only be explained in the present model by enhanced injection of electrons, which become *the majority carriers for more than one self-assembled layer* ($x > 1$). Thus, the injection of electrons and holes can be controlled and balanced by the thickness of the self-assembled anode functionalization layer. The increase of the layer thickness increases the hole injection barrier and simultaneously reduces the barrier for electron injection. The optimally efficient thickness for device performance is reached when those barriers are comparable in magnitude. For the case of an ITO/$(SiO_2)_x$/TPD/AlQ/Al device, this optimum thickness is ∼1 nm ($x = 1$).

As discussed, the aforementioned effects are more pronounced for the Al cathode device, which possesses a larger energy barrier to electron injection than the Mg cathode and therefore would benefit more from mechanisms that aid electron injection. For similar reasons, the effect on the maximum quantum efficiency in the Mg cathode devices is also diminished.

Conclusions

Chlorosilyl self-assembly techniques effect the self-limiting deposition of conformal, contiguous, smooth, microstructurally well-characterized dielectric layers on the surface of ITO anodes used for OLED devices. These layers can be deposited with Angstrom-level control of film thickness to form relatively pinhole-free films. Insertion of these films at the anode−HTL interface of OLED structures dramatically enhances the quantum and luminous efficiencies of such devices and affords significant insight into the fluence of hole injection at the anode−HTL interface, especially when Al is used as the cathode. This increase in efficiency and accompanying turn-on voltage effects can be associated with several competing factors: (1) balance between the fluence of injected holes and electrons achieved via attenuation of majority carrier (hole) injection, (2) alteration of the ITO work function and the ITO surface Fermi level relative to the HTL HOMO, (3) creation of an internal "built-in" field that enhances electron injection fluence from the cathode.

Acknowledgment. We thank ONR through the Center for Advanced Multifunctional Nonlinear Optical Polymers and Molecular Assemblies (CAMP) MURI (N00014-95-1-1319) and the NSF-MRSEC program through the Northwestern Materials Research Center (DMR-0076097) for support of this research. J.G.C.V. thanks NSERC of Canada for a postdoctoral fellowship. We thank Dr. V. Rassolov for help with the electronic structure calculations.

Supporting Information Available: Atomic force micrograph; forward light output vs current density plots for ITO/$(SiO_2)_x$/TPD (600 Å)/Alq (600 Å)/M (M = Al, Mg) devices; Figures S1, S2, and S3 (PDF). This material is available free of charge via the Internet at http://pubs.acs.org.

CM020293Q

(41) Kong, J.; White, C. A.; Krylov, A. I.; Sherrill, D.; Adamson, R. D.; Furlani, T. R.; Lee, M. S.; Lee, A. M.; Gwaltney, S. R.; Adams, T. R.; Ochsenfeld, C.; Gilbert, A. T. B.; Kedziora, G. S.; Rassolov, V. A.; Maurice, D. R.; Nair, N.; Shao, Y. H.; Besley, N. A.; Maslen, P. E.; Dombroski, J. P.; Daschel, H.; Zhang, W. M.; Korambath, P. P.; Baker, J.; Byrd, E. F. C.; Van Voorhis, T.; Oumi, M.; Hirata, S.; Hsu, C. P.; Ishikawa, N.; Florian, J.; Warshel, A.; Johnson, B. G.; Gill, P. M. W.; Head-Gordon, M.; Pople, J. A. Q-Chem 2.0: A High-Performance ab initio Electronic Structure Program Package. *J. Comput. Chem.* **2001**, *21*, 1532−1548.

(42) $\epsilon = 4$ has been shown to be an appropriate value for the dielectric constant of SiO_2 layers when thicknesses exceed 1.3 nm: (a) Ahmed, K.; Ibok, E.; Bains, G.; Chi, D.; Ogle, B.; Wortman, J. J.; Hauser, J. R. *IEEE Trans. Electron. Devices* **2000**, *47*, 1349−1354. (b) Green, M. L.; Sorsch, T. W.; Timp, G. L.; Muller, D. A.; Weir, B. E.; Silverman, P. J.; Moccio, S. V.; Kim, Y. *Microelectron. Eng.* **1999**, *48*, 25−30. Thus, $\epsilon = 4$ is appropriate for the present system and affords quantitative information when the number of monolayers exceeds one and reasonable qualitative information for a single monolayer.

(43) This decrease is nonmonotonic as noted previously. This behavior may be understood as the consequence of the saturation of the interface layer dipole moment and of the built-in voltage. Such saturation is a reasonable result of the strong electrostatic interactions between the molecular dipoles within the layers.